Gas Permeation Properties of Silica Membranes with Uniform Pore Sizes Derived from Polyhedral Oligomeric Silsesquioxane

Masakoto Kanezashi
Dept. of Chemical Engineering, Hiroshima University, Higashi-Hiroshima 739-8527, Japan

Takahiro Shioda, and Takahiro Gunji
Dept. of Pure and Applied Chemistry, Tokyo University of Science, Noda 278-8510, Japan

Toshinori Tsuru
Dept. of Chemical Engineering, Hiroshima University, Higashi-Hiroshima 739-8527, Japan

DOI 10.1002/aic.12716
Published online July 20, 2011 in Wiley Online Library (wileyonlinelibrary.com).

The sol-gel method was applied in the fabrication of homogenous polyhedral oligomeric silsesquioxane (HOMO-POSS)-derived silica membranes. Single gas permeation characteristics in a temperature range of 100–500°C were examined to discuss the effect of silica precursor on amorphous silica networks. HOMO-POSS-derived membranes showed a CO_2 permeance of 1.1 × 10^{-7} mol m^{-2} s^{-1} Pa^{-1} with a CO_2/CH_4 permeance ratio of 131 at 100°C, which is a superior CO_2/CH_4 separation performance by comparison with tetraethoxysilane (TEOS)-derived silica membranes. Normalized Knudsen-based permeance (NKP) was applied for quantitative evaluation of pore size. HOMO-POSS-derived membranes had loose amorphous silica structures compared to TEOS-derived membranes and pore size was successfully tuned by changing the calcination temperatures. The activation energy for a HOMO-POSS-derived membrane fired at 550°C with a uniform pore size of ∼ 0.42 nm increased linearly with the ratio of the kinetic diameter of the gas molecule to the pore diameter, λ (=d_k/d_p), and showed a trend similar to that of DDR-type zeolite membranes. © 2011 American Institute of Chemical Engineers *AIChE J,* 58: 1733–1743, 2012
Keywords: sol-gel method, membrane, amorphous silica, gas permeation, CO_2 separation

Introduction

Zeolites are crystalline aluminosilicate materials with micropores (zeolitic pores) in their structures. They are built up by various connections of TO_4 (T = Si or Al) tetrahedral units, which result in various zeolitic pore sizes and structures.[1–3] As zeolite channel size and surface chemistry (hydrophobicity, hydrophilicity) can be controlled by the Si/Al ratio in the framework, various types of zeolite membranes, for example, large-pore (Y-type,[4,5] MOR[6,7]), medium-pore (ZSM-5[8–11]), and small-pore (A-type,[12] SAPO-34,[13–15] and DDR[16,17]) zeolite membranes, have been prepared and used for gas separation and pervaporation. However, the presence of intercrystalline gaps in a membrane degrades the separation performance of zeolitic pores, so the zeolite layer, which is active in separation, needs to be thick enough to prevent the formation of intercrystalline gaps. A large number of studies seeking the fabrication of a thin zeolite layer with fewer intercrystalline gaps are in progress.

Compared to zeolite membranes, it has been reported that amorphous silica membranes derived by chemical vapor deposition (CVD) and the sol-gel method show high hydrogen separation performance, due to a very thin active separation layer with an average pore size of ∼ 0.3 nm.[18–22] The sol-gel method is generally much more flexible for control of the pore size of amorphous silica membranes. There are two ways to control silica membrane pore size: the polymeric sol-gel route and the colloidal sol-gel route.[23] The polymeric route for the control of pore size is preferable in the preparation of gas separation membranes, since colloidal sol-gel route, in which spaces between colloidal particles are assumed to be pores in a membrane, it is very difficult to control the spaces to the level of several angstroms. For the polymeric route, pore size is thought to be made up of spaces within amorphous silica networks, which consist of random networks containing 3-, 4-, 5-, 6-, 7-, and 8-membered siloxane rings.[24] An amorphous silica structure, prepared by molecular-dynamics simulation, was recently reported to have a negligible number of pores larger than 0.35 nm.[25] The pore sizes of these silica membranes are appropriate to separate hydrogen (kinetic diameter: 0.289 nm) from small molecules such as N_2 (kinetic diameter: 0.364 nm) and CH_4 (0.38 nm), but appear to be small for the separation of, for example, CO_2/CH_4, H_2/organic gas mixtures and C_3 isomers. Thus, the appropriate design and control of pore size for amorphous silica structures would be a breakthrough for the practical application of silica membranes.

An organic-template approach was applied by several research groups to control amorphous silica network sizes.[26–32]

Correspondence concerning this article should be addressed to M. Kanezashi at kanezashi@hiroshima-u.ac.jp, and T. Tsuru at tsuru@hiroshima-u.ac.jp.

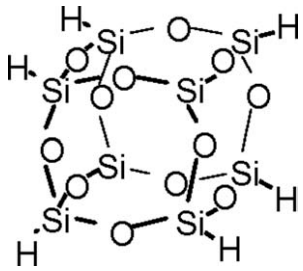

Figure 1. Molecular structure of polyhedral oligomeric silsesquioxane (POSS).

The concept for the control of pore size by the organic-template method is as follows. Organic groups in silica gels derived from copolymerization of TEOS, which is a commonly used precursor for silica membranes, and alkyltriethoxysilane having methyl and/or phenyl groups, will burn out after pyrolysis in an air atmosphere and leave pores, i.e., the size and shape of the pores in a membrane can be determined by the size and shape of the organic groups. Inorganic networks prepared using amorphous silica with pyrolysis of methyl groups in air gave high CO_2 permeance, on the order of $\sim 10^{-7}$ mol m^{-2} s^{-1} Pa^{-1}, with CO_2/CH_4 selectivity higher than 70.[26] Kusakabe et al.[28] also investigated the effect of the length of alkyl groups on pore structure as well as the permeation properties of silica membranes, which were prepared by copolymerization of TEOS and octyl-, dodecyl-, or octadecyltriethoxysilane. Another advantage of utilization of organic-inorganic hybrid alkoxides is improved hydrothermal stability of amorphous silica membrane.[30–32] Methylated microporous silica membranes were successfully fabricated by acid-catalyzed sol-gel hydrolysis and condensation of a mixture of TEOS and MTES.[30,32] The incorporation of methyl groups in microporous silica membranes with controlled silica network size was proven to enhance the service time in the dehydration of a butanol-water mixture from a few weeks to more than 18 months (water flux: 4 kg m^{-2} h^{-1} with selectivity 500–20,000).[30] Duke et al.[31] also reported the improved hydrothermal stability of the carbonized silica membrane because carbon templates block the micropore spaces, thereby inhibiting the silanol migration and condensation that leads to micropore closure.

Recently, we proposed a ''spacer'' technique to control the pore sizes of silica membranes using a bridged alkoxide, which consists of organic functional groups between two silicon atoms. Hybrid silica membranes derived by bis (triethoxysilyl) ethane (BTESE, Si—C—C—Si unit structure) showed H_2 permeance approximately one order of magnitude higher ($\sim 10^{-5}$ mol m^{-2} s^{-1} Pa^{-1}), compared with previously reported TEOS-derived silica membranes (single Si unit structure), and a high H_2 to SF_6 permeance ratio ($\sim$ 20,000) with a low H_2 to N_2 selectivity ($\sim$ 20).[33,34] Pore size distribution, as determined by single-gas permeation, showed BTESE-derived silica membranes had loose amorphous silica structures compared with TEOS-derived silica membranes due to the differences in the minimum units of the silica networks. These results suggest that changes in the minimum units can control the average pore size of amorphous silica networks.

Polyhedral oligomeric silsesquioxane (POSS), which has a cage structure consisting of $(RSiO_{3/2})_8$ (R=H or organic groups) units and a well-defined nanometer-sized structure, is one of the most attractive nano building blocks (NBB) for the preparation of advanced nanocomposites (Figure 1).[35] They are usually prepared by careful hydrolysis of the corresponding trifunctional silicanes.[36–38] Only a few papers have reported on the gas permeation properties of polymer membranes with POSS particles incorporated (mixed-matrix membranes) for membrane fabrication.[39–41] Dasgupta et al.[40] reported that the gas permeability of CH_4, N_2, O_2, and CO_2 through POSS-polyimide nanocomposite membranes increased significantly with comparable selectivity, due to an increase in the fractional volume caused by the bulky POSS cages within the polymer. However, no work has been published on the fabrication and gas permeation properties of silica membranes fabricated using pure components of POSS. This article reports on the synthesis of homogeneous (HOMO)-POSS-derived silica membranes by the sol-gel method and their single gas permeation characteristics in the temperature range of 100–500°C. Normalized Knudsen-based permeance (NKP) for the determination of membrane pore sizes less than 1 nm,[42] which is based on the gas translation model originally proposed by Xiao and Wei[43] and Shelekhin et al.,[44] was applied for quantitative evaluation of the pore size of HOMO-POSS-derived silica membranes prepared at various temperatures.

Experimental

Preparation of HOMO-POSS-derived silica sol and membrane fabrication

HOMO-POSS-derived silica sol was prepared by dehydrogenation and polymerization of polyhedral oligomeric silsesquioxane $(HSiO_{3/2})_8$ (0.30 g, 0.71 mmol) with H_2O in a mixed solvent of tetrahydrofuran (THF) (30 ml) and benzene (40 ml) under N_2 atmosphere (POSS/H_2O molar ratio: 1/8).[38] *N,N*-diethylhydroxylamine (1 μl, 9.7 μmol) was added as a catalyst, and the mixture was stirred at 0°C for 90 min. The solvent was then removed by evaporation under reduced pressure, followed by the addition to THF to prepare a coating sol of 0.5 wt %.

Porous α-alumina tubes (porosity: 50%; average pore size: 1 μm; outside diameter: 10 mm) were used as supports for the HOMO-POSS-derived silica membranes. α-alumina particles (average particle diameter: 0.2, 1.9 μm) were coated on the outer surface of a porous support using silica-zirconia colloidal sol as the binder, and the support was fired at 550°C for 30 minutes to make the surface smooth. These procedures were repeated several times to cover large pores that might result in pinholes in the final membrane. Then, SiO_2—ZrO_2 (Si/Zr = 1/1) sol diluted to about 0.5 wt % was coated on the substrate to form an intermediate layer with pore sizes of several nm.[22,33,34] After coating, the membrane was fired at 550°C for about 30 min. Finally, the HOMO-POSS-derived silica layer was fabricated by coating with the HOMO-POSS sol, followed by drying and calcination at 300 and 550°C, respectively, in air for 30 min.

Single gas permeation measurement

Figure 2 shows a schematic diagram of the experimental apparatus for single gas permeation measurement. A single gas of industrial grade (He, H_2, CO_2, N_2, CH_4, SF_6) was fed on the outside of the membrane at atmospheric pressure, while the permeate side (downstream) was evacuated by a vacuum pump. The permeation cell was kept at a given temperature between 100 and 500°C. The permeances were calculated from the observed pressure difference across the membrane and the permeation rate, which was obtained by a

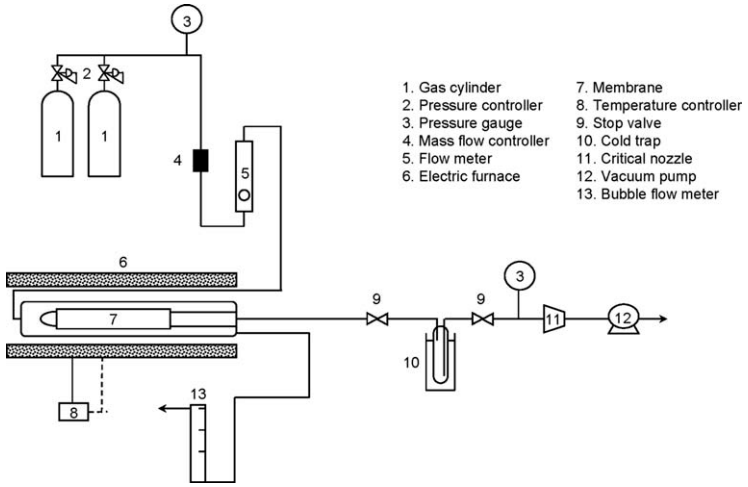

Figure 2. Schematic diagram of experimental apparatus for gas permeation measurement.

calibrated critical nozzle placed between the permeation cell and the vacuum pump.[45]

Results and Discussion

Characteristics of a HOMO-POSS-derived silica membrane

Figure 3 shows the SEM image of the cross section of a HOMO-POSS-derived membrane. Although it is quite difficult to distinguish the silica layer from the SiO_2—ZrO_2 intermediate layer with an average pore size of approximately 1–2 nm, as measured by nanopermporometry,[46] a thin continuous silica separation layer can be seen on the top and/or inside of the SiO_2—ZrO_2 intermediate layer. The thickness of the active separation layer was clearly less than 1 μm. Figure 4 shows the inverse of H_2 permeance for a HOMO-POSS-derived membrane fired at 300°C as a function of the number of sol coats applied. It should be noted that 0 coats indicates the membrane performance of the SiO_2—ZrO_2 intermediate layer. There are two types of slopes for the inverse of H_2 permeance as a function of the number of coats. The inverse of H_2 permeance increased greatly by the third coat, and after that increased slightly with additional coats, while the H_2/SF_6 permeance ratio increased linearly by five coats and approached a constant of $\sim$ 1000. The H_2/CO_2 permeance ratio showed $\sim$ 5.8 despite the number of sol coats and was almost same as Knudsen selectivity (4.69). This is because molecular sieving effect between H_2 and CO_2 was not sufficient due to smaller molecular size of CO_2 (kinetic diameter: 0.33 nm) than SF_6 (kinetic diameter: 0.55 nm). This indicates that HOMO-POSS-derived membrane fired at 300°C seems to be suitable for separation of H_2 from organic gas mixtures rather than H_2/CO_2 separation. In the case of no penetration of HOMO-POSS-derived sol to the inside of the intermediate layer, which corresponds to layer-by-layer coating, the permeation resistance, which can be expressed with the inverse of H_2 permeance, increased linearly without changing slope. So Figure 3 shows that some HOMO-POSS-derived polymers seemed to penetrate into the intermediate layer. It is preferable, for improved gas permeability of a membrane, to prevent the penetration of sol into the intermediate layer, so further studies are now in progress to optimize the coating properties of HOMO-POSS polymer (molecular weight, polymer structure) as well as the average pore size of the intermediate layer. In the present study, a HOMO-POSS-derived silica membrane was fabricated by coating five times with HOMO-POSS-derived sol (molecular weight: 30,000 g mol^{-1} [38]).

Estimation of average pore size of HOMO-POSS-derived silica membranes

The pore size distribution of porous silica membranes was estimated by measuring several gas permeances at 200°C.

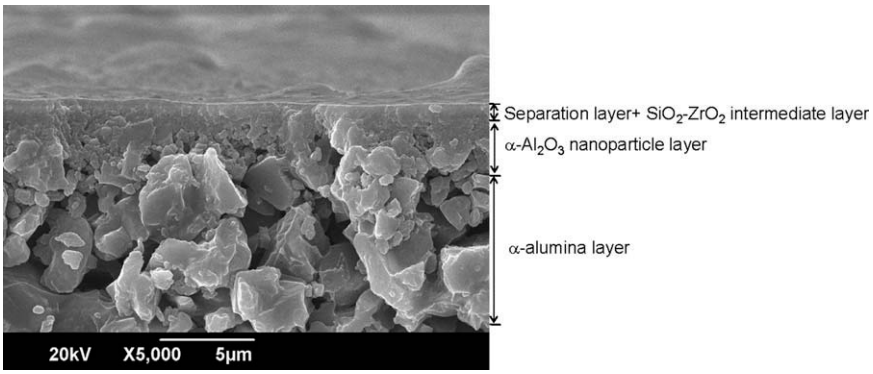

Figure 3. SEM image of a cross section of a HOMO-POSS-derived silica membrane.

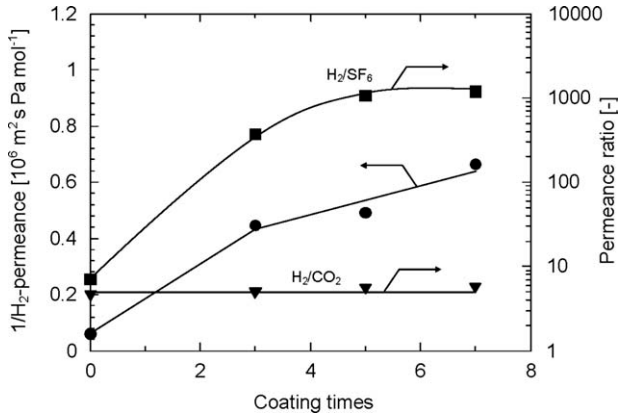

Figure 4. Inverse of H_2-permeance, H_2/SF_6 and H_2/CO_2 permeance ratio at 200°C for a HOMO-POSS-derived silica membrane fired at 300°C as a function of the number of coats.

Figure 5 shows gas permeances at 200°C for HOMO-POSS-derived and TEOS-derived silica membranes fabricated by firing at 300 and 550°C as a function of kinetic diameter. A HOMO-POSS-derived membrane fired at 300°C showed high hydrogen permeance of 2.0×10^{-6} mol m^{-2} s^{-1} Pa^{-1} with a high H_2/SF_6 permeance ratio of 1200 and a low H_2/N_2 permeance ratio ($\sim$ 20) at 200°C. On the other hand, a TEOS-derived membrane fired at 300°C showed H_2 permeance one order of magnitude lower than that of a HOMO-POSS-derived silica, with a moderate permeance ratio of H_2 to CH_4 ($\sim$ 60). It should be noted that the permeance of SF_6 was less than 10^{-10} mol m^{-2} s^{-1} Pa^{-1}, which is the detection limit of this gas permeation system. The permeance of gases with a molecular size larger than CO_2 (kinetic diameter: 0.33 nm) for a HOMO-POSS-derived membrane fired at 550°C were one to two orders of magnitude smaller than for those fired at 300°C, resulting in a slight decrease in H_2 permeance with an increased H_2/CH_4 permeance ratio of 1000. A TEOS-derived membrane fired at 550°C[46] showed gas permeances one to two orders of magnitude smaller with a molecular size larger than H_2 (kinetic diameter: 0.289 nm), in comparison with those fired at 300°C, resulting in highly selective of H_2 to N_2. These results suggest that firing at 550°C shifted the pore size distribution of both membranes (TEOS-derived[46] and HOMO-POSS-derived) to a smaller size, in comparison with firing at 300°C, due to sintering of the amorphous silica structure (condensation of Si—OH groups).

Recently, we proposed a modified gas translation model and derived NKP for the determination of pore sizes less than 1 nm[42] based on an original proposal by Xiao and Wei[43] and Shelekhin.[44] NKP is the ratio of permeance of the i-th component to that predicted for the j-th component under the Knudsen diffusion mechanism, expressed as Eq. 1.

$$\mathrm{NKP} = \frac{P_i}{P_j}\frac{\sqrt{M_i}}{\sqrt{M_j}} = \frac{P_i}{P_{\mathrm{He}}\sqrt{M_{\mathrm{He}}/M_i}} \tag{1}$$

When He, the smallest molecule, is taken as a reference (j-th component), $P_{\mathrm{He}}\sqrt{M_{\mathrm{He}}/M_i}$ is the permeance of the i-th component predicted from He permeance under the Knudsen diffusion mechanism, and therefore, NKP corresponds to the ratio of experimentally obtained permeance to predicted permeance based on He. It should be noted that NKP equals 1 for the Knudsen mechanism, and NKP indicates how much the experimentally obtained permeance is decreased due to the molecular sieving effect. The gas translation (GT) or activated Knudsen diffusion model was derived for diffusion through microporous inorganic membranes using probability, ρ_i.

$$P_i = \varepsilon_i d_{\mathrm{p}} \rho_i \sqrt{\frac{8RT}{\pi M_i}} \frac{1}{RT\tau_i L_i} \tag{2}$$

Membrane structural factors (pore size, porosity, tortuosity, thickness) are expressed as d_{p}, ε_i, τ_i, and L_i. Since the probability, ρ_i, is expressed in Eq. 3 with the pre-exponential, $\rho_{\mathrm{g},i}$, and the kinetic energy, $E_{\mathrm{p},i}$, to overcome the diffusion barrier, the permeance in Eq. 2 can be expressed in Eq. 4.

$$\rho_i = \rho_{\mathrm{g},i} \exp\left(-\frac{E_{\mathrm{p},i}}{RT}\right) \tag{3}$$

$$P_i = \varepsilon_i d_{\mathrm{p}} \rho_{\mathrm{g},i} \sqrt{\frac{8RT}{\pi M_i}} \frac{1}{RT\tau_i L_i} \exp\left(-\frac{E_{\mathrm{p},i}}{RT}\right) = \frac{k_0}{\sqrt{M_i RT}} \exp\left(-\frac{E_{\mathrm{p},i}}{RT}\right) \tag{4}$$

where $k_0 = \frac{\varepsilon_i d_{\mathrm{p}} \rho_{\mathrm{g},i}}{\tau_i L_i}\sqrt{\frac{8}{\pi}}$ is the structural parameter. Equation 4 covers the activated diffusion ($E_{\mathrm{p},i} > 0$), surface diffusion ($E_{\mathrm{p},i} < 0$) and Knudsen diffusion ($E_{\mathrm{p},i} = 0$). The activation energy can be determined by interactions between permeating molecules and the pore wall, based on the Lennard-Jones potential using the size (membrane pore size, molecular size of permeating molecules) and the interaction parameters. Because $\rho_{\mathrm{g},i}$, which is the probability of the i-th component at an infinite kinetic energy, corresponds to the geometrical probability, that is, the effective area for permeation, it can be defined by the following equation.

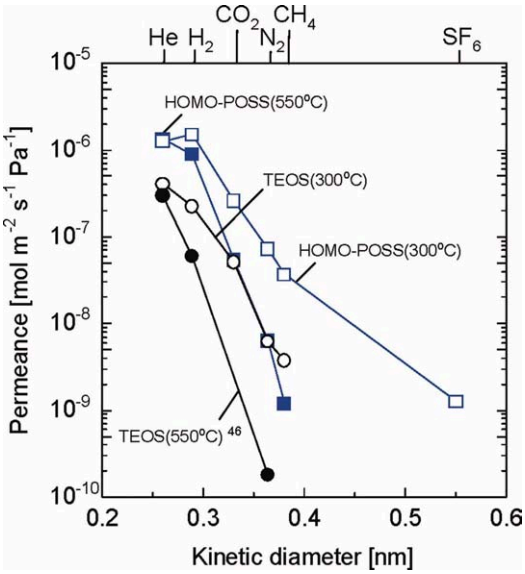

Figure 5. Gas permeances at 200°C for HOMO-POSS-derived silica and TEOS-derived silica membranes fired at 300 and 550°C as a function of kinetic diameter.

[Color figure can be viewed in the online issue, which is available at wileyonlinelibrary.com.]

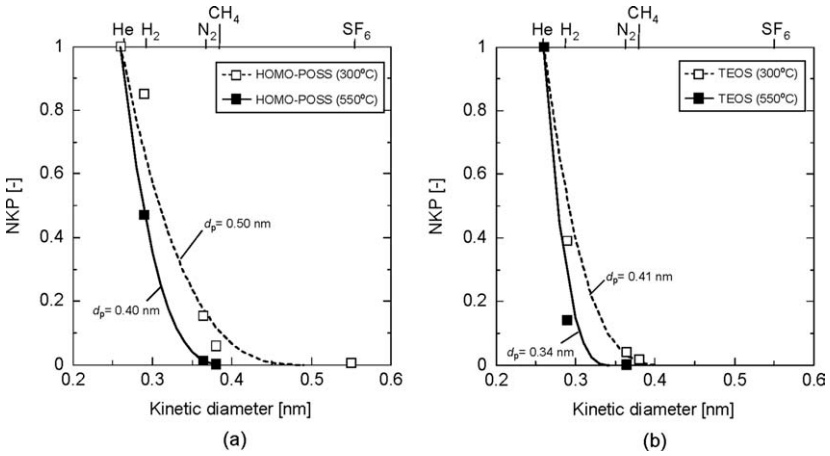

Figure 6. NKP plot at 200°C as a function of kinetic diameter; symbols are experimental, and curves are calculated based on Eq. 10 for HOMO-POSS-derived silica (a) and TEOS-derived silica (b).

$$\rho_{g,i} = \frac{1}{3}\frac{A_i}{A_0} \tag{5}$$

where A_i is the area of the pore opening for effective permeation of the i-th component, and A_0 is the cross-sectional area of the pore. The GT model assumes no structural size of permeating molecules, so k_0 is independent of any permeating molecules, that is, the k_0 of a large gas such as SF_6 is exactly the same as a small gas such as He. In the modified GT model, the diffusion distance in Eqs. 2 and 4 is assumed to be $(d_p - d_{k,i})$ instead of d_p for the i-th component (molecular size: $d_{k,i}$), since the center of the i-th component cannot approach the wall. Therefore, A_i, the area of the pore opening effective for diffusion, is proportional to the effective pore area, which leads to the modified GT model as follows (Eq. 7).

$$\rho_g = \frac{1}{3}\frac{A_i}{A_0} = \frac{1}{3}\frac{\pi(d_p - d_{k,i})^2/4}{\pi d_p^2/4} = \frac{1}{3}\frac{(d_p - d_{k,i})^2}{d_p^2} \tag{6}$$

$$P_i = \frac{\varepsilon_i}{3\tau_i L_i}(d_p - d_{k,i})\frac{(d_p - d_{k,i})^2}{d_p^2}\sqrt{\frac{8}{\pi M_i RT}}\exp\left(-\frac{E_{p,i}}{RT}\right) \tag{7}$$

Based on the discussion above, which is quite similar to the derivation of Ferry's equation commonly used and accepted for the analysis of solute permeation in ultrafiltration, the following expression for NKP can be obtained.

$$\begin{aligned}\mathrm{NKP} &= \frac{P_i}{P_{He}}\frac{\sqrt{M_i}}{\sqrt{M_{He}}} = \frac{k_{0,i}}{k_{0,He}}\cdot\exp\left(-\frac{E_{P,i} - E_{P,He}}{RT}\right) \\ &= \frac{(d_p - d_{k,i})^3}{(d_p - d_{k,He})^3}\cdot\exp\left(-\frac{E_{p,i} - E_{p,He}}{RT}\right)\end{aligned} \tag{8}$$

It should be noted that membrane structural factors, such as tortuosity, τ_i, and membrane thickness, L_i, are rationally assumed to be the same irrespective of the molecule, due to a cylindrical pore structure. Equation 8 indicates that NKP can be expressed with the configurational factors (pore size d_p, molecular size $d_{k,i}$) and the activation energy of the permeances of He and the i-th component, which require a set of experimental data on the temperature dependence of permeances. Once $k_{0,i}$ and $E_{p,i}$ are obtained by fitting a set of experimental data on the temperature dependence of permeances with Eq. 7, one can derive the following equation, which consists of configurational parameters (pore size d_p, molecular size of permeating molecules, $d_{k,He}$, $d_{k,i}$) and corresponds to NKP at infinite temperature.

$$\frac{k_{0,i}}{k_{0,He}} = \frac{(d_p - d_{k,i})^3}{(d_p - d_{k,He})^3} \tag{9}$$

In this section, for simplicity, the assumption has been made that the activation energies, $E_{p,i}$, are the same for any type of gas, to easily evaluate the pore sizes of microporous membranes, leading to the following expression for NKP.

$$\mathrm{NKP} = \frac{(d_p - d_{k,i})^3}{(d_p - d_{k,He})^3} \tag{10}$$

Figure 6 shows the NKP plot at 200°C for HOMO-POSS-derived (a) and TEOS-derived (b) silica membranes fired at 300 and 550°C, respectively, as a function of kinetic diameter. It should be noted that NKP for CO_2 molecules was not plotted, due to adsorption by silica even at 200°C. Pore size, d_p, was estimated by fitting experimentally obtained NKP with Eq. 10. Judging from fitted curves based on Eq. 10 for HOMO-POSS and TEOS-derived silica membranes, the order of pore size can be estimated as follows: TEOS-derived silica fired at 550°C (0.34 nm) < HOMO-POSS-derived silica fired at 550°C (0.40 nm) < TEOS-derived silica fired at 300°C (0.41 nm) < HOMO-POSS-derived silica membrane fired at 300°C (0.50 nm). A high H_2/N_2 permeance ratio can be attained by membranes with an average pore size of 0.35 nm, while a high H_2/SF_6 permeance ratio can be attained by membranes with a much larger average pore size (0.50 nm). HOMO-POSS-derived silica membranes showed larger pore sizes than TEOS-derived silica membranes, despite different calcination temperatures (300 and 550°C). The reason for the larger pore size of HOMO-POSS-derived silica than TEOS-derived silica can be attributed to the minimum unit of amorphous silica networks. Figure 7 shows a schematic image of amorphous silica networks derived from TEOS (a) and POSS (b). For amorphous silica networks derived from POSS, POSS can be the minimum unit. In this case, the intercubic pores formed by covalent linking of siloxane cage compounds via Si—O—Si bonds are the pores

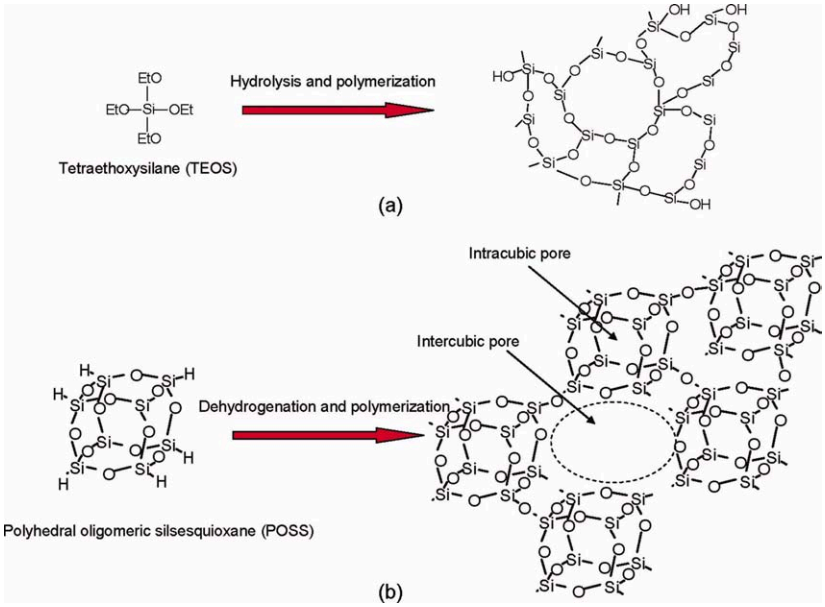

Figure 7. Schematic images of amorphous silica networks derived by TEOS (a) and POSS (b).

[Color figure can be viewed in the online issue, which is available at wileyonlinelibrary.com.]

through which gas molecules can permeate, because the intracubic pores are too small for hydrogen molecules to permeate.[47] In conclusion, the spaces formed from POSS were confirmed to be much larger than that those formed from TEOS, due to the larger minimum unit of amorphous silica networks.

Temperature dependence of gas permeance for HOMO-POSS-derived silica membranes

Figure 8a shows the temperature dependence of gas permeance in the temperature range of 100–300°C for a HOMO-POSS-derived silica membrane fired at 300°C. The permeances of H_2 and CH_4 were approximately independent of temperature. The permeance of He increased slightly with increasing temperature, while the permeance of N_2 and SF_6 increased with decreasing temperature (Knudsen-like permeation behavior). Similar temperature dependence was reported in a silica membrane with a larger average pore size.[34] It is thought that the permeation behavior of He and H_2 through amorphous silica networks strongly depends on the average pore size and pore size distribution of amorphous silica networks. When the pore size of silica networks is close to He and H_2 in molecular size, these molecules can permeate via an activated permeation mechanism (gas permeance increases with an increase in temperature), i.e., the permeance of He is higher than that of H_2 due to its smaller molecular size. On the other hand, when the pore size of the silica network is much larger than the molecular size of He and H_2, He and H_2 can permeate by the Knudsen permeation mechanism (gas permeance increases with a decrease in temperature), i.e., the permeance of H_2 is higher than that of He due to its smaller molecular weight. Therefore, He and H_2 permeation behavior can be governed by the balance of flow through activated and/or Knudsen permeation, depending on the ratio of molecular size to pore size of an amorphous silica network. The HOMO-POSS-derived silica membrane seems to be mostly controlled by Knudsen selectivity through loose silica network pores for small molecules, and by molecular sieving for large molecules (moderate H_2/N_2 permeance ratio: 20; high H_2/SF_6 permeance ratio: 1000). The permeance of CO_2 increased with decreasing temperature because of higher adsorption of CO_2 on the silica surface at a lower temperature, due to a strong affinity in comparison with other gases.

Figure 8b shows the temperature dependence of gas permeance in the temperature range of 100–500°C for a HOMO-POSS-derived membrane fired at 550°C. The permeance of SF_6 was below the detection limit of the permeation equipment ($<10^{-10}$ mol m^{-2} s^{-1} Pa^{-1}). The permeances of He, H_2, N_2, and CH_4 greatly increased with increasing temperature, which is the activated permeation mechanism. The H_2/CH_4 permeance ratio was higher than 300 in this temperature range and increased with decreasing temperature, because CH_4 permeance is more temperature-dependent than H_2 permeance. The permeation tendency of CO_2 molecules was similar to that fired at 300°C, i.e., the permeance of CO_2 increased greatly with decreasing temperature, giving a larger CO_2/CH_4 permeance ratio of 131 with high permeance of 10^{-7} mol m^{-2} s^{-1} Pa^{-1} even at 100°C. Most papers have reported Knudsen permeation of N_2 and CH_4 molecules for H_2 permselective membranes, because these molecules can only permeate through pinholes created by the large size of siloxane rings and/or spaces between colloidal particles.[46] However, a HOMO-POSS-derived membrane fired at 550°C showed activated permeation behavior of N_2 and CH_4 molecules that can be achieved by uniform pores with fewer pinholes (sharp pore size distribution).[48,49] Thus, the formation of a uniform pore size is possible in the case of calcination at 550°C for a HOMO-POSS derived membrane.

The activation energy and membrane structural factor k_0 were obtained by regressing Eq. 4 with the experimental single permeation data above 100°C for a membrane fired at 300°C and above 300°C for one fired at 550°C, and are summarized in Table 1. CO_2 was not calculated because surface diffusion may contribute greatly to permeation due to an adsorption effect between the CO_2 molecules and the silica structure below 300°C. It should be noted that the pre-exponential term, k_0, which indicates the structural factors of

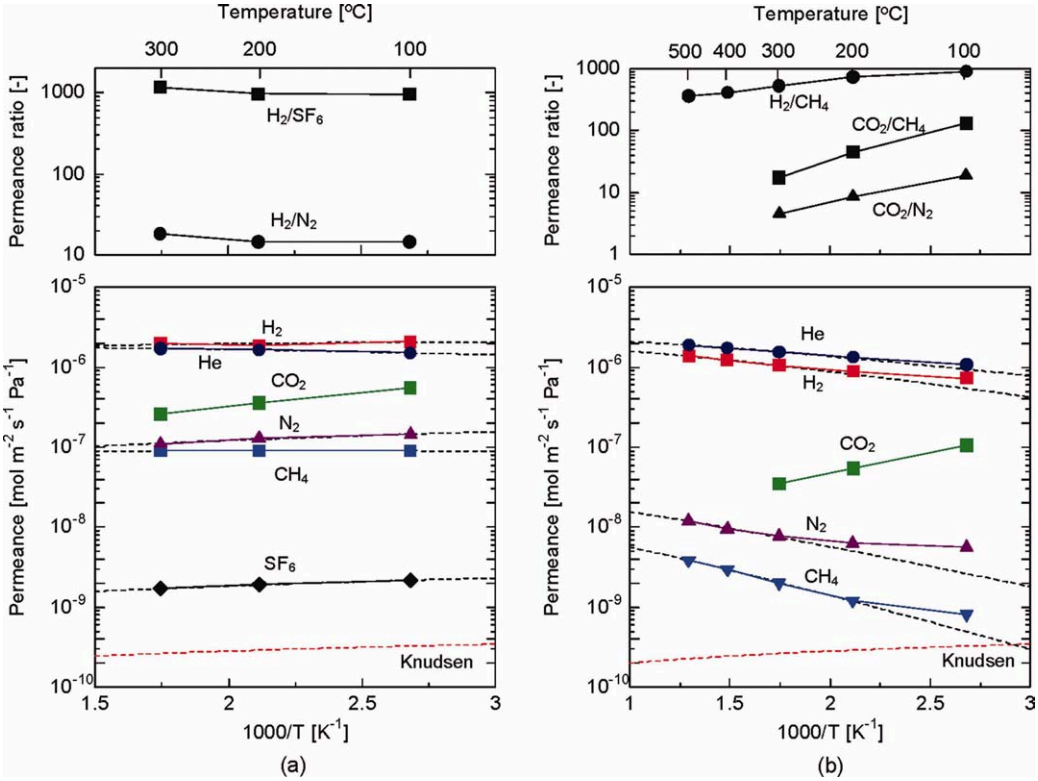

Figure 8. Temperature dependence of gas permeances for HOMO-POSS-derived silica membranes fired at 300°C (a) and at 550°C (b) (broken curves fitted with Eq. 4).

[Color figure can be viewed in the online issue, which is available at wileyonlinelibrary.com.]

amorphous silica networks, only reflects the pore structure, including pore area and volume, in the amorphous silica. According to the GT model, $k_0 = \frac{\varepsilon_i d_p \rho_{g,i}}{\tau_i L_i}\sqrt{\frac{8}{\pi}}$ is independent of any permeating molecules. However, Table 1 shows that the value of k_0 decreased with increased molecular size for both membranes, suggesting that the GT model (Eq. 4), which assumes constant diffusion distance, d_p, for any type of gas, is not applicable to the present permeation data.

Figure 9 shows the $k_{0,i}/k_{0,He}$ ratio, which corresponds to NKP at infinite temperature, for HOMO-POSS-derived membranes fired at 300°C (a) and 550°C (b), as a function of kinetic diameter. It should be noted that the predicted curves for $d_p = 0.50$ and $d_p = 0.40$ nm for membranes fired at 300 and 550°C, respectively, obtained by Eq. 10, are also shown in the figure as dotted curves. Judging from the fitted curves using the $k_{0,i}/k_{0,He}$ ratio for HOMO-POSS-derived silica membranes, pore size can be estimated as 0.49 nm for HOMO-POSS-derived silica fired at 300°C and 0.42 nm for HOMO-POSS-derived silica fired at 550°C, indicating no large difference in comparison with that obtained by Eq. 10. This is because the fitted curves were obtained without the NKP plot of CO_2, which is an adsorptive gas, as shown in Figure 8. Lee et al.[42] reported that in the case of verification of this model by DDR-type zeolite, which has a defined channel size of 0.36 × 0.44 nm, the NKP plot for CO_2 decreased from 4.97 to 0.72 with an increase in permeation temperatures from 100 to 400°C due to a decrease in the contribution of surface diffusion at high temperatures, and the calculated curve for $d_p = 0.44$ nm showed good agreement with experimental data measured at higher temperatures.

Table 1. Activation Energy and Pre-exponential Parameters (k_0) Fitted with Eq. (4)

Membrane	Gas	k_0 (−)	E_p (kJ mol^{-1})
HOMO-POSS-derived silica fired at 300°C	He	4.51×10^{-4}	3.06
	H_2	2.51×10^{-4}	1.39
	N_2	3.75×10^{-5}	0.42
	CH_4	3.71×10^{-5}	1.89
	SF_6	1.37×10^{-6}	0.21
HOMO-POSS-derived silica fired at 550°C	He	8.19×10^{-4}	6.38
	H_2	5.25×10^{-4}	7.79
	N_2	2.88×10^{-5}	11.2
	CH_4	1.17×10^{-5}	14.5

Analysis of the pore size of HOMO-POSS-derived silica membranes by activation energy

The activation energy of gas permeation, which is calculated as the interaction between permeating molecules and the pore wall in a membrane, can be a good indicator for the evaluation of pore size where gas molecules can permeate, i.e., activation energy increases with smaller pore size because of a larger repulsive force.[24] Figure 10 shows the He/H_2 permeance ratio and H_2 permeance at 300°C as a function of the activation energy of H_2 permeation of HOMO-POSS-derived silica fired at 300 and 550°C, as well as sol-gel[34,50] and CVD-derived[21,51–54] silica membranes (Bis (triethoxysilyl) ethane (BTESE)-derived, TEOS-derived, and Tetramethylorthosilicate (TMOS)-derived). The upper part of this figure shows H_2 permeances for HOMO-POSS-, BTESE-, TEOS-, and TMOS-derived silica membranes at 300°C. A correlation between the He/H_2 permeance ratio and the activation energy of H_2 permeation was obtained,

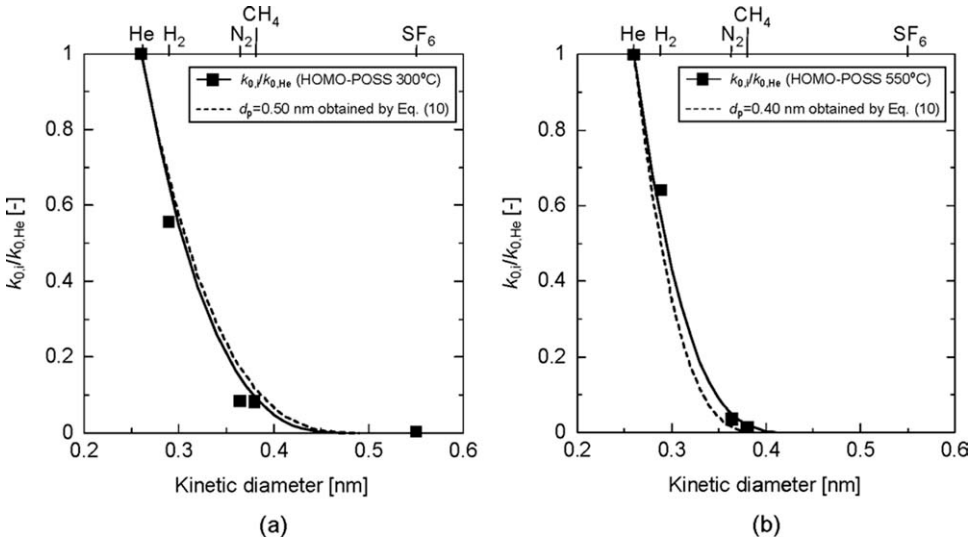

Figure 9. $k_{0,i}/k_{0,He}$ ratio as a function of kinetic diameter; symbols are experimental, and curves are calculated based on Eq. 8 (solid curve) and Eq. 10 (dotted curve), respectively, for HOMO-POSS-derived silica membrane fired at 300°C (a) and at 550°C (b).

despite the different silica precursors (TEOS, TMOS, BTESE, HOMO-POSS) and different membrane fabrication methods (sol-gel, CVD). It should be noted that the He/H_2 permeance ratio, which indicates the pore size distribution of the amorphous structures that He and H_2 molecules can permeate, increased with increasing activation energy of H_2 permeation. Sol-gel derived silica membranes (TEOS) after exposure to steam (500°C; partial pressure of steam: 300–400 kPa)[50] showed much larger activation energy with larger He/H_2 permeance ratios, due to the densification of amorphous silica networks, than those without exposure to steam.[21,51–54] A HOMO-POSS-derived silica membrane fired at 300°C showed activation energy with a small He/H_2 permeance ratio, similar to BTESE-derived silica membranes, confirming much looser amorphous networks than TEOS-derived silica. On the other hand, HOMO-POSS-derived membranes fired at 550°C showed much larger activation energy with larger He/H_2 permeance ratios than those fired at 300°C, which is consistent with the membrane pore size predicted by the NKP plot. The H_2 permeance of a HOMO-POSS-derived silica membrane fired at 300°C was comparable to that of BTESE-derived silica, and decreased with increasing activation energy due to the decrease in the pore size of the silica membranes.

As shown in Table 1, the activation energy of a membrane fired at 550°C increased as molecular size increased. Similar trends were reported in silica and modified zeolite membranes.[48,49,55] Kanezashi et al.[55] reported that for high quality DDR-type zeolite membranes, the activation energy of diffusion increased as the size of the permeating gases increased (He: 6.66 kJ mol^{-1}<H_2: 9.62 kJ mol^{-1}<CO_2: 12.8 kJ mol^{-1}<CO: 15.5 kJ mol^{-1}) under conditions of negligible adsorption (at temperatures above 300°C). The high temperature diffusion data for small gases in the DDR-type zeolites, measured by the macroscopic membrane permeation method, are consistent with the theory of translational gas diffusion in zeolites proposed by Xiao and Wei.[43] That is, for small gases with weak adsorption affinity with zeolites, molecules in the zeolite pores retain their gas characteristics and must overcome the energy barrier imposed by the zeolite pore structure. Therefore, the activation energy depends strongly on the ratio of the kinetic diameter of the diffusion gas molecule to the zeolite pore diameter, λ ($=d_k/d_p$).[43]

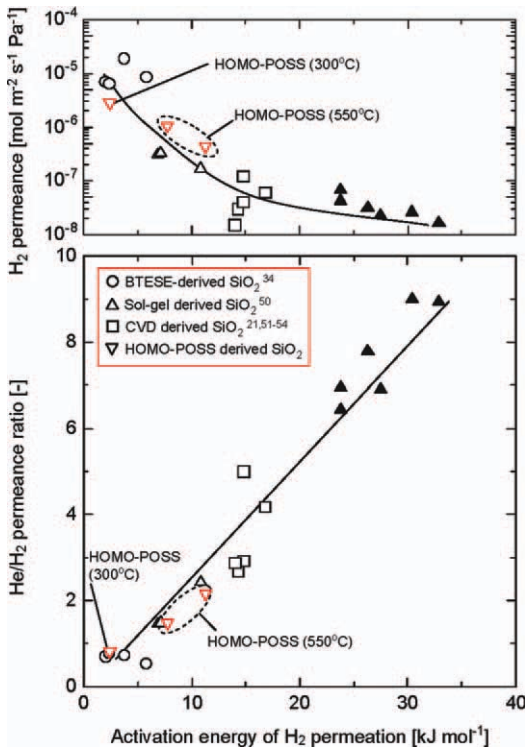

Figure 10. He/H_2 permeance ratio and H_2 permeance at 300°C as a function of activation energy of H_2 permeation for HOMO-POSS-derived silica fired at 300 and 550°C as well as sol-gel[34,50] and CVD-derived[21,51–54] silica membranes (BTESE-derived, TEOS-derived, TMOS-derived) (closed symbols: membrane performance after exposure to steam; open symbols: membrane performance without exposure to steam).

[Color figure can be viewed in the online issue, which is available at wileyonlinelibrary.com.]

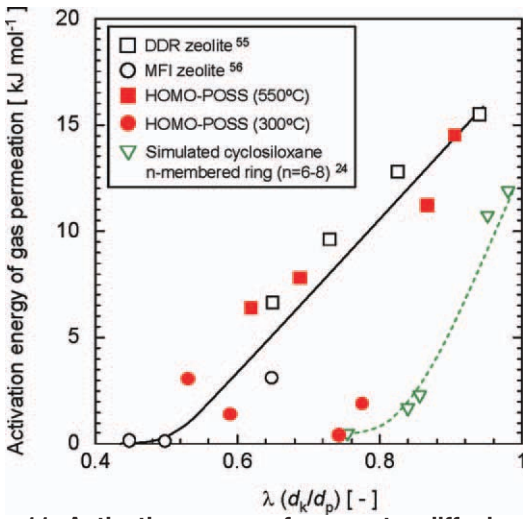

Figure 11. Activation energy for counter-diffusion CVD modified DDR-type (open square symbols),[55] MFI-type (open circle symbols)[56] zeolite, and HOMO-POSS-derived membranes fired at 300°C (closed circle symbols) and 550°C (closed square symbols), as well as simulated cyclosiloxane *n*-membered rings (n = 6–8),[24] as a function of the ratio of the kinetic diameter of a gas molecule to a pore diameter λ ($=d_k/d_p$).

[Color figure can be viewed in the online issue, which is available at wileyonlinelibrary.com.]

Figure 11 compares the activation energy of counter-diffusion CVD-modified DDR-type (open square symbols),[55] MFI-type (open circle symbols)[56] zeolite, and HOMO-POSS-derived membranes fired at 300°C (closed circle symbols) and 550°C (closed square symbols), as well as simulated cyclosiloxane n-membered rings (n = 6–8),[24] as a function of the ratio of the kinetic diameter of the gas molecules to the pore diameter λ ($=d_k/d_p$). For the calculation of λ for HOMO-POSS-derived membranes, d_p = 0.49 nm was used for the membrane fired at 300°C and d_p = 0.42 nm was used for that fired at 550°C (values obtained by Eq. 8). The activation energy of DDR-type zeolite membranes was larger than those of MFI-type zeolite membranes, due to the smaller zeolite channels of the former type. The activation energy increased approximately linearly with λ ($=d_k/d_p$) of above 0.5. Even though some experimental data was scattered, the activation energy of HOMO-POSS-derived silica membranes also increased linearly with λ ($=d_k/d_p$), and a membrane fired at 550°C showed values similar to those of DDR-type zeolite membranes, due to similar pore size. These results suggest that a HOMO-POSS-derived silica membrane fired at 550°C has a uniform pore size of $\sim$ 0.42 nm with a negligible number of pinholes. The formation of a uniform pore size in the case of calcination at high temperatures using a POSS is probably due to the uniform size of the minimum unit of a POSS, which has a stable structure even at high temperatures. The activation energy data of He and H_2 permeation through $H_{2n}Si_nO_n$ (n = 6–8) cyclosiloxane n-membered rings by ab initio calculation[24] were also plotted as a function of λ in the same figure, confirming a similar tendency with different absolute values. Direct comparison of the absolute values of the activation energy obtained by the permeation experiments with the simulation might be difficult, because the absolute value calculated from the permeation data depends on membrane structural factors such as overlap of the permeation path, but the latter was only calculated as the interaction between permeating molecules and one cyclosiloxane *n*-membered ring without thermal vibration. However, it is important to show a similar trend, that is, the activation energy that increased with λ ($=d_k/d_p$).

HOMO-POSS-derived silica membranes fired at 550°C were expected to show gas separation performance similar to that of DDR-type zeolite membranes, which are one of the candidates for the separation of CO_2/CH_4 mixtures. Table 2 summarizes CO_2 permeance and the CO_2/CH_4 permeance ratio for HOMO-POSS-derived silica as well as inorganic membranes (SAPO-34,[13–15] DDR-type zeolite,[16,17] TEOS-derived silica,[26,29,57,58] and carbon[59]). It should be noted that all the data in this table were obtained by single gas permeation. In general, the CO_2/CH_4 permeance ratio decreases with increasing CO_2 permeance due to the trade-off relationships. The scattered CO_2/CH_4 permeance ratios for TEOS-derived silica membranes probably result from the difficulty of precise control of the pore size for the separation of CO_2 and CH_4 molecules. High CO_2 separation performance can be seen in both zeolite membranes (DDR-type, SAPO-34) at 25°C, due to the high molecular-sieving effect and adsorption by the appropriate zeolite channel size. The permeance of CO_2 and the CO_2/CH_4 permeance ratio for both zeolite membranes decreased greatly as temperature increased (25–100°C), due to the permeation mechanism of CO_2 by surface diffusion. HOMO-POSS-derived silica membranes fired at 550°C showed approximately the same CO_2 permeance ($\sim 4.0 \times 10^{-7}$ mol m^{-2} s^{-1} Pa^{-1}) and CO_2/CH_4 permeance ratio ($\sim$ 131) at 100°C as DDR-type zeolite membranes at 100°C. High CO_2 separation performance at 100°C of HOMO-POSS-derived silica membranes was achieved by molecular

Table 2. CO_2 Permeance and CO_2/CH_4 Permeance Ratio for HOMO-POSS-Derived Silica as well as Inorganic Membranes (SAPO-34,[13–15] DDR-Type Zeolite,[16,17] TEOS-Derived Silica,[26,29,57,58] Carbon [59])

Temperature (°C)	Membrane Material	CO_2 Permeance (10^{-7} mol m^{-2} s^{-1} Pa^{-1})	CO_2/CH_4 Permeance Ratio (–)	Literature Cited
100°C	HOMO-POSS	1.1	131	This work
		3.7	67	
		1.0	68	
		3.1	64	
	SAPO-34	0.6	12	13
		0.6	18	14
	DDR zeolite	0.8	80	16
		1.0	100	17
25°C	SAPO-34	1.5	20	13
		1.1	23	14
		3.6	227	15
	DDR zeolite	2.9	422	16
		3.3	183	16
		0.8	400	17
		4.4	600	17
	TEOS-derived SiO_2	0.7	72	26
		10	10	29
		60	6	54
		0.2	30	55
	Carbon	0.026	127	56
		0.068	102	56

sieving effect rather than adsorption by uniform pore size of amorphous silica and a thin active separation layer.

Conclusions

The sol-gel method was applied for the fabrication of HOMO-POSS-derived silica membranes. A thin, continuous silica separation layer for selective gas separation was successfully formed on a silica-zirconia intermediate layer. Single gas permeation characteristics in the temperature range of 100–500°C were examined to determine the effect of the silica precursor on amorphous silica networks. NKP for the determination of membrane pore sizes less than 1 nm was applied for quantitative evaluation of the pore size of HOMO-POSS-derived silica membranes prepared at various temperatures.

(1) HOMO-POSS-derived silica membranes had loose amorphous silica structures compared to TEOS-derived silica membranes, due to the difference in the minimum unit of silica networks, and pore size was successfully tuned by changing the calcination temperatures. A HOMO-POSS-derived membrane fired at 300°C showed high hydrogen permeance of 2.0×10^{-6} mol m^{-2} s^{-1} Pa^{-1} with a high H_2/SF_6 permeance ratio of 1200 and a low H_2/N_2 permeance ratio ($\sim$ 20) at 200°C. A HOMO-POSS-derived membrane fired at 550°C showed permeances of gases with molecular sizes larger than CO_2 (kinetic diameter: 0.33 nm) that were one to two orders of magnitude smaller than the membrane fired at 300°C, resulting in a slight decrease in H_2 permeance with an increased H_2/CH_4 permeance ratio of $\sim$ 1000.

(2) A correlation between He/H_2 permeance ratio and activation energy of H_2 permeation was obtained, despite different silica precursors (TEOS, TMOS, BTESE, HOMO-POSS) and different membrane fabrication methods (sol-gel, CVD), i.e., He/H_2 permeance ratio increased with increasing activation energy of H_2 permeation. HOMO-POSS-derived membranes fired at 550°C showed much higher activation energy with larger He/H_2 permeance ratios, in comparison with those fired at 300°C, which was consistent with the membrane pore size predicted by the NKP plot.

(3) The activation energy of a HOMO-POSS-derived silica membrane fired at 550°C increased linearly with the ratio of the kinetic diameter of the gas molecule to the pore diameter, λ ($=d_k/d_p$), under conditions of negligible adsorption, and showed values similar to those of DDR-type zeolite membranes. These results suggest that a HOMO-POSS-derived silica membrane fired at 550°C has a uniform pore size of $\sim$ 0.42 nm, which was predicted by the NKP plot.

(4) HOMO-POSS-derived silica membranes showed approximately the same CO_2 permeance ($\sim 4.0 \times 10^{-7}$ mol m^{-2} s^{-1} Pa^{-1}) and CO_2/CH_4 permeance ratio ($\sim$ 131) at 100°C as those for DDR-type zeolite membranes at 100°C, which are one of the candidates for the separation of CO_2/CH_4 mixtures. High CO_2 separation performance can be achieved by uniform pore size of the amorphous silica and a thin active separation layer.

Notation

A_i = area of the pore opening for effective permeation of i-th component, m^2
A_0 = cross-sectional area of the pore, m^2
$d_{k,i}$ = molecular size of the i-th component, m
d_p = pore diameter, m
E_p = kinetic energy, J mol^{-1}
$k_{0,i}$ = structural parameter of i-th component, dimensionless
L = membrane thickness, m
M = molecular weight, g mol^{-1}
NKP = normalized Knudsen-based permeance, dimensionless
P = permeance, mol m^{-2} s^{-1} Pa^{-1}
R = gas constant, J mol^{-1} K^{-1}
T = temperature, K

Greek letters

ε = membrane porosity, dimensionless
λ = the ratio of kinetic diameter of the gas molecules to the pore diameter, dimensionless
τ = tortuosity, dimensionless
ρ = probability, dimensionless
$\rho_{g,i}$ = probability of i-th component, dimensionless

Literature Cited

1. Caro J, Noack M, Kölsch P, Schäfer R. Zeolite membranes-state of their development and perspective. *Microporous Mesoporous Mater*. 2000;38:3–24.
2. Lin YS, Kumakiri I, Nair BN, Alsyouri H. Microporous inorganic membranes. *Sep Purif Method*. 2002;31:229–379.
3. Bowen TC, Noble RD, Falconer JL. Fundamentals and applications of pervaporation through zeolite membranes. *J Membr Sci*. 2004;245:1–33.
4. Kusakabe K, Kuroda T, Murate A, Morooka S. Formation of a Y-type zeolite membrane on a porous α-alumina tube for gas separation. *Ind Eng Chem Res*. 1997;36:649–655.
5. Li SG, Tuan VA, Noble RD, Falconer JL. Pervaporation of water/THF mixtures using zeolite membranes. *Ind Eng Chem Res*. 2001;40:4577–4585.
6. Nishiyama N, Uemiya K, Matsukata M. A defect free mordenite membrane synthesized by vapor phase transport method. *J Chem Soc Chem Commun*. 1995;1967–1968.
7. Tavolaro A, Julbe A, Guizard C, Basile A, Cot L, Drioli E. Synthesis and characterization of a mordenite membrane on an α-Al_2O_3 tubular support. *J Mater Chem*. 2000;10:1131–1137.
8. Yan Y, Davis ME, Gavalas GR. Preparation of zeolite ZSM-5 membranes by in-situ crystallization on porous α-Al_2O_3. *Ind Eng Chem Res*. 1995;34:1652–1661.
9. Lovallo MC, Tsapatsis M. Preferentially oriented submicron silicalite membranes. *AIChE J*. 1996;42:3020–3029.
10. Hedlund J, Noack M, Kölsch P, Creaser D, Caro J, Sterte J. ZSM-5 membranes synthesized without organic templates using a seeding technique. *J Membr Sci*. 1999;159:263–273.
11. Yuan W, Lin YS, Yang W. Molecular sieving MFI-type zeolite membranes for pervaporation separation of xylene isomers. *J Am Chem Soc*. 2004;126:4776–4777.
12. Kita H, Horii K, Ohtoshi Y, Tanaka K, Okamoto K. Synthesis of a zeolite NaA membrane for pervaporation of water/organic liquid mixtures. *J Mater Sci Lett*. 1995;14:206–208.
13. Poshusta JC, Tuan VA, Pape EA, Noble RD Falconer JL. Separation of light gas mixtures using SAPO-34 membranes. *AIChE J*. 2000;46:779–789.
14. Li S, Falconer JL, Noble RD. SAPO-34 membranes for CO_2/CH_4 separation. *J Membr Sci*. 2004;241:121–135.
15. Carreon MA, Li S, Falconer JL, Noble RD. SAPO-34 seeds and membranes prepared using multiple structure directing agents. *Adv Mater*. 2008;20:729–732.
16. Himeno S, Tomita T, Suzuki K, Nakayama K, Yajima K, Yoshida S. Synthesis and permeation properties of a DDR-type zeolite membrane for separation of CO_2/CH_4 gaseous mixtures. *Ind Eng Chem Res*. 2007;46:6989–6997.
17. van den Bergh J, Tihaya A, Kapteijn F. High temperature permeation and separation characteristics of an all-silica DDR zeolite membrane. *Micropor Mesopor Mater*. 2010;132:137–147.
18. Gavalas GR, Megris CE, Nam SW. Deposition of H_2-permselective SiO_2 films. *Chem Eng Sci*. 1989;44:1829–1835.
19. de Vos RM, Verweij H. High-selectivity,high-flux silica membranes for gas separation. *Science* 1998;279:1710–1711.

20. Ockwig NW, Nenoff TM. Membranes for hydrogen separation. *Chem Rev*. 2007;107:4078–4110.
21. Gu Y, Oyama ST. High molecular permeance in a poreless ceramic membrane. *Adv Mater*. 2007;19:1636–1640.
22. Kanezashi M, Yamamoto A, Yoshioka T, Tsuru T. Characteristics of ammonia permeation through porous silica membranes. *AIChE J*. 2010;56:1204–1212.
23. Brinker CJ, Sehgal R, Hietala SL, Deshpande RD, Smith DM, Loy D, Ashley CS. Sol-gel strategies for controlled porosity inorganic materials. *J Membr Sci*. 1994;94:85–102.
24. Hacarlioglu P, Lee D, Gibbs GV, Oyama ST. Activation energy for permeation of He and H_2 through silica membranes: An ab initio calculation study. *J Membr Sci*. 2008;313:277–283.
25. Yoshioka T, Asaeda M, Tsuru T. A molecular dynamics simulation of pressure-driven gas permeation in a microporous potential field on silica membranes. *J Membr Sci*. 2007;293:81–93.
26. Raman NK, Brinker CJ. Organic "template" approach to molecular sieving silica membranes. *J Membr Sci*. 1995;105:273–279.
27. Cao G, Lu Y, Delattre L, Brinker CJ, López GP. Amorphous silica molecular sieving membranes by sol-gel processing. *Adv Mater*. 1996;8:588–591.
28. Kusakabe K, Sakamoto S, Saie T, Morooka S. Pore structure of silica membranes formed by a sol-gel technique using tetraethoxysilane and alkyltriethoxysilanes. *Sep Purif Technol*. 1999;16:139–146.
29. Xomeritakis G, Naik S, Braunbarth CM, Cornelius CJ, Pardey R, Brinker CJ. Organic-templated silica membranes I. Gas and Vapor transport properties. *J Membr Sci*. 2003;215:225–233.
30. Campaniello J, Engelen CWR, Haije WG, Pex PPAC, Vente JF. Long-term pervaporation performance of microporous methylated silica membranes. *Chem Commun*.2004:834–835.
31. Duke MC, da Costa JCD, Do DD, Gray PG, Lu GQ. Hydrothermally robust molecular sieving silica for wet gas separation. *Adv Funct Mater*. 2006;16:1215–1220.
32. Castricum HL, Sah A, R. Kreiter, Mittelmeijer-Hazeleger MC, Huiskes C, ten Elshof JE. Microporous structure and enhanced hydrophobicity in methylated SiO_2 for molecular separation. *J Mater Chem*. 2007;17:1509–1517.
33. Kanezashi M, Yada K, Yoshioka T, Tsuru T. Design of silica networks for development of highly permeable hydrogen separation membranes with hydrothermal stability. *J Am Chem Soc*. 2009;131:414–415.
34. Kanezashi M, Yada K, Yoshioka T, Tsuru T. Organic-inorganic hybrid silica membranes with controlled silica network size: preparation and gas permeation characteristics. *J Membr Sci*. 2010;348:310–318.
35. Baney RH, Itoh M, Sakakibara A, Suzuki T. Silsesquioxanes. *Chem Rev*. 1995;95:1409–1430.
36. Morris RE. Modular materials from zeolite-like building blocks. *J Mater Chem*. 2005;15:931–938.
37. Hagiwara Y, Shimojima A, Kuroda K. Alkoxysilylated-derivatives of double-four ring silicate as novel bulding blocks of silica-based materials. *Chem Mater*. 2008;20:1147–1153.
38. Kajiwara T, Shioda T, Abe Y, Gunji T. Synthesis of novel polysiloxanes containing polyhedral octasilsesquioxanes and their properties. *World J Eng*. 2009;6:451–452.
39. Ríos-Dominguez H, Ruiz-Treviño FA, Contreras-Reyes R, González-Montiel A. Syntheses and evaluation of gas transport properties in polystyrene-POSS membranes. *J Membr Sci*. 2006;271:94–100.
40. Dasgupta B, Sen SK, Banerjee S. Aminoethylaminopropylisobutyl POSS-polyimide nanocomposite membranes and their gas transport properties. *Mater Sci Eng B*. 2010;168:30–35.
41. Li F, Li Y, Chung TS, Kawi S. Facilitated transport by hybrid POSS®-Matrimid®-Zn^{2+} nanocomposite membranes for the separation of natural gas. *J Membr Sci*. 2010;356:14–21.
42. Lee HR, Kanezashi M, Shimomura Y, Yoshioka T, Tsuru T. Evaluation and fabrication of pore-size-tuned silica membranes with tetraethoxydimethyl disiloxane for gas separation. *AIChE J*. DOI 10.1002/aic.12501.
43. Xiao J, Wei J. Diffusion mechanism of hydrocarbons in zeolites—I. *Theory, Chem Eng Sci*. 1992;47;1123–1141.
44. Shelekhin AB, Dixon AG, Ma YH. Theory of gas diffusion and permeation in inorganic molecular-sieve membranes. *AIChE J*. 1995;41:58–67
45. Kanezashi M, Asaeda M. Hydrogen permeation characteristics and stability of Ni-doped silica membranes in steam at high temperature. *J Membr Sci*. 2006;271:86–93.
46. Tsuru T. Nano/subnano-tuning of porous ceramic membranes for molecular separation. *J Sol-Gel Technol*. 2008;46:349–361.
47. Sheng YJ, Lin WJ, Chen WC. Network structures of polyhedral oligomeric silsesquioxane based nanocomposites: a monte carlo study. *J Chem Phys*. 2004;121:9693–9701.
48. de Vos RM, Verwij H. Improved performance of silica membranes for gas separation. *J Membr Sci*. 1998;143:37–51.
49. Diniz da Costa JC, Lu GQ, Rudolph V, Lin YS. Novel molecular sieve silica (MSS) membranes: characterisation and permeation of single-step and two-step sol-gel membranes. *J Membr Sci*. 2002;198:9–21.
50. Kanezashi M, Asaeda M. Stability of H_2-permeselective Ni-doped silica membranes in steam at high temperature. *J Chem Eng Jpn*. 2005;38:908–912.
51. Hwang GJ, Onuki K, Shimizu S, Ohya H. Hydrogen separation in H_2-H_2O-HI gaseous mixture using the silica membrane prepared by chemical vapor deposition. *J Membr Sci*. 1999;162:83–90.
52. Lee D, Oyama ST. Gas permeation characteristics of a hydrogen selective supported silica membrane. *J Membr Sci*. 2002;210:291–306.
53. Araki S, Mohri N, Yoshimitsu Y, Miyake Y. Synthesis, characterization and gas permeation properties of a silica membrane prepared by high-pressure chemical vapor deposition. *J Membr Sci*. 2007;290:138–145.
54. Nagano T, Fujisaki S, Sato K, Hataya K, Iwamoto Y, Nomura M, Nakao SI. Relationship between the mesoporous intermediate layer structure and the gas permeation property of an amorphous silica membrane synthesized by counter diffusion chemical vapor deposition. *J Am Ceram Soc*. 2008;91:71–76.
55. Kanezashi M, O'Brien-Abraham J, Lin YS, Suzuki K. Gas permeation through DDR-type zeolite membranes at high temperatures. *AIChE J*. 2008;54:1478–1486.
56. Kanezashi M, Lin YS. Gas permeation and diffusion characteristics of MFI-type zeolite membranes at high temperatures. *J Phys Chem C* 2009;113:3767–3774.
57. Yoshioka T, Nakanishi E, Tsuru T, Asaeda M. Experimental study of gas permeation through microporous silica membranes. *AIChE J*. 2001;47:2052–2063.
58. Xomeritakis G, Tsai CY, Brinker CJ. Microporous sol-gel derived aminosilicate membrane for enhanced carbon dioxide separation. *Sep Purif Technol*. 2005;42:249–257.
59. Yoshimune M, Fujiwara I, Haraya K. Carbon molecular sieve membranes derived from trimethylsilyl substituted poly(phenylene oxide) for gas separation. *Carbon* 2007;45:553–560.

Manuscript received Apr. 5, 2011, and revision received Jun. 6, 2011.